# Comparison of the Stream Structure and Coronal Sources of the Solar Wind During the April 7 & May 12, 1997 Halo CMEs

C. N. Arge[1], G. de Toma[2], and J. G. Luhmann[3]

[1]*Space Vehicles Directorate/AFRL, Hanscom AFB, Massachusetts, USA*

[2]*NCAR/HAO, CU/CIRES, and NOAA/SEC, Boulder, Colorado, USA*

[3]*SSL/University of California Berkeley, Berkeley, California, USA*

**Abstract.**     We report on our efforts to model the ambient solar wind out to 1AU around the times of the April 7 and May 12, 1997 halo coronal mass ejections (CMEs) and to identify their coronal source regions. We use the simple physics and empirical based Wang-Sheeley-Arge (WSA) model driven by daily updated photospheric field synoptic maps from Mount Wilson Solar Observatory to accomplish this. The results generated by the WSA model for each event are then compared with the WIND satellite observations near Earth, as well as with SOHO/EIT data. We find that the model describes the observed ambient solar wind stream structure of the May 12 CME generally well, except for the ejecta itself. The same is essentially true for the April 7 event, except that in this case it fails to capture the moderately high-speed ambient stream that followed behind the CME ejecta.

## 1.   Introduction

The April 7 and May 12, 1997 halo CMEs occurred shortly after solar minimum when solar activity was low and the structure of the corona and solar wind was relatively simple. The April 7 event was associated with active region NOAA AR 8027, which was positioned $\sim30°$ south and $\sim20°$ east of central meridian. The May 12 event was associated with the only active region (NOAA AR 8038) on the solar disk at the time, which was located $\sim20°$ north of the equator near central meridian. Both regions had new cycle polarity. The flare associated with the April 7 event began at 1350 UT and peaked at 1407 UT (Berdichevsky et al., 1998), while the May 12 event was associated with the only major flare of the day, which began at 0442 UT and peaked around 0455 UT (Webb et al. 2000a,b). Both events were flanked by twin dimming regions and were associated with filament eruptions and EIT waves (Webb et al., 2000a).

The April 7 halo CME was observed in the SOHO/LASCO C2 instrument at 1427 UT with an estimated frontal speed of between 600-800 km/s (Berdichevsky et al., 1998) and onset time of approximately 1400 UT. The shock produced by the interplanetary coronal mass ejection (ICME) arrived at L1 at 1255 UT on April 10 followed by a magnetic cloud-like feature and then a high-speed stream (Berdichevsky et al., 1998, Webb et al., 2000a). A moderate geomagnetic storm with a maximum $Dst$ of -82 nT resulted from the ICME. The May 12 halo CME was observed in the LASCO C2 instrument at 0630 UT with an estimated frontal

speed of ~600km/s (Plunkett et al., 1998) and onset time between 0430-0500 UT. The shock produced by the ICME arrived at L1 early on the 15th followed by a magnetic cloud and then a high-speed stream, which is speculated (Webb et al., 2000b) to have compressed the cloud from behind. The ICME produced a moderate geomagnetic storm with a maximum $Dst$ of -115nT.

The April and May events are very similar to each other in their basic properties (i.e., slow, ambient solar wind for many days prior to the eruption of a halo CME, followed by an ICME, and then a moderate high-speed stream). We attempt to model the ambient solar wind out to 1AU around the times of these two CME events and to identify their coronal source regions. The objective is to establish how well we can do this and to determine what can be learned when the modeling fails to reproduce the observations. If we are to ever realistically model the propagation and evolution of CMEs, we must first be able to reliably model and predict the structure of the ambient solar wind, as it is the medium through which they propagate. We use the simple physics and empirical based Wang-Sheeley-Arge (WSA) model driven by daily updated photospheric field synoptic maps from Mount Wilson Solar Observatory (MWO) to do this. To understand our findings we compare in detail WSA modeling results, solar observations, and solar wind data at L1.

## 2.   Wang-Sheeley-Arge (WSA) Model

The Wang-Sheeley-Arge (WSA) model is a combined empirical and physics based representation of the quasi-steady global solar wind flow. It can be used to predict the ambient solar wind speed and interplanetary magnetic field (IMF) polarity at Earth. It is an improved version of the original Wang and Sheeley model (Wang & Sheeley 1992). It uses ground-based line-of-sight (LOS) observations of the Sun's surface magnetic field as input to a magnetostatic potential field source surface (PFSS) model (Schatten, Wilcox, & Ness 1969; Altschuler & Newkirk, 1969), which determines the coronal field out to 2.5 solar radius (Rs). The output of the PFSS model serves as input to the Schatten Current Sheet (SCS) model (Schatten, 1971), which provides a more realistic magnetic field topology of the upper corona. The following empirical relationship developed by Arge et al. (2003 & 2004) is used to assign solar wind speed at a radius of 5Rs (for this study).

$$V(f_s, \theta_b) = 265 + \frac{1.5}{(1+f_s)^{2/7}} \left\{ 5.7 - 1.3e^{[1-(\theta_b/4.3)^2]} \right\}^{3.5} \text{ km s}^{-1} \qquad (1)$$

It is a function of two coronal parameters, flux tube expansion factor ($f_s$) and the minimum angular separation (at the photosphere) between an open field footpoint and its nearest coronal hole boundary ($\theta_b$). The empirically derived solar wind speeds and magnetic field values at 5Rs from the SCS model are then fed into a 1-D modified kinematic code (Arge & Pizzo 2000) that propagates the solar wind out to 1AU and accounts for stream interactions. A more comprehensive summary of the WSA model is provided in Arge et al. (2004).
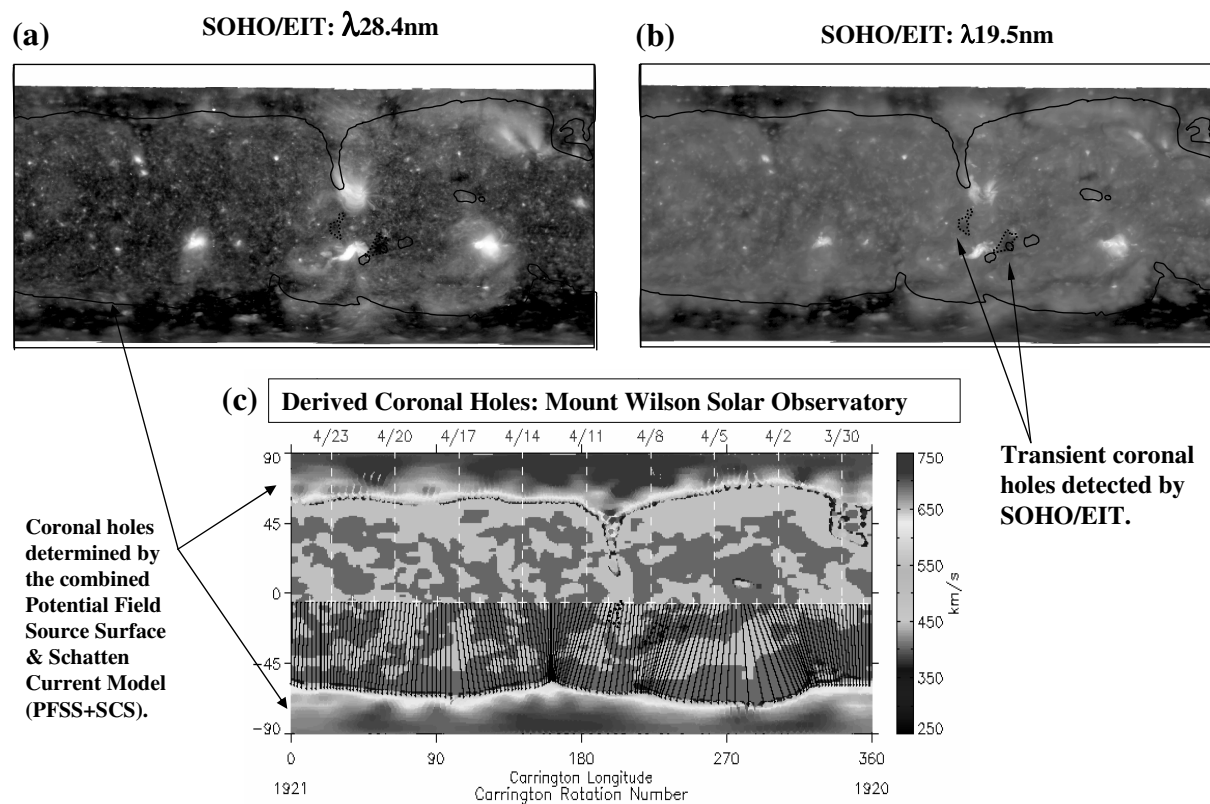
**(a)** SOHO/EIT: λ28.4nm

**(b)** SOHO/EIT: λ19.5nm

**(c)** Derived Coronal Holes: Mount Wilson Solar Observatory

Transient coronal holes detected by SOHO/EIT.

Coronal holes determined by the combined Potential Field Source Surface & Schatten Current Model (PFSS+SCS).

Figure 1.    (a) SOHO\EIT 28.4nm & (b) 19.5nm synoptic maps for CR1921. (c) Coronal holes as determined by the PFSS+SCS model for CR1921. The field polarity at the photosphere is indicated by the light (positive polarity) and dark (negative polarity) gray contours, while the gray dots identify the footpoints of the open field lines (i.e., the coronal holes) at the photosphere. The white plus signs near the equator mark the daily positions of the sub-earth point at the beginning of each day indicated. The black straight lines identify the connectivity between the outer (open) boundary located at 5Rs and the source regions of the solar wind at the photosphere. The outlines of the predicted coronal holes have been placed on top of Fig. 1a & 1b
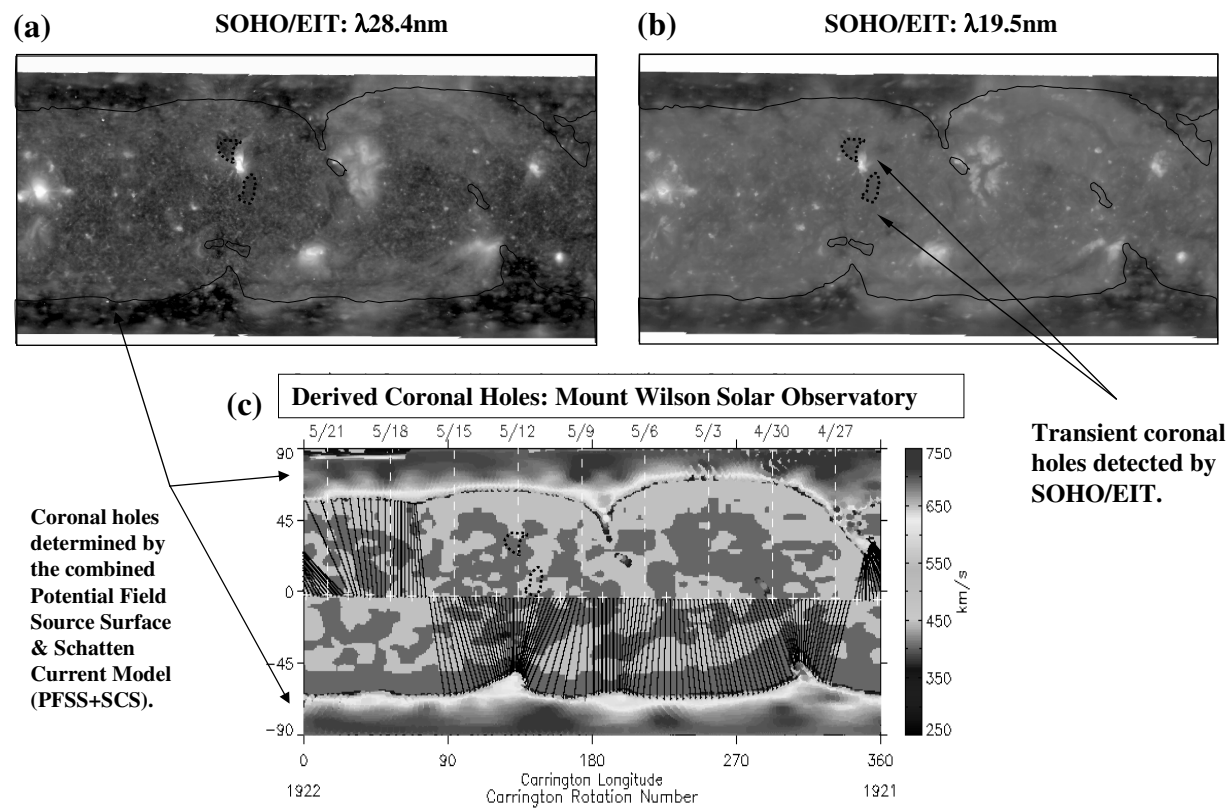
**(a)** **SOHO/EIT: λ28.4nm**

**(b)** **SOHO/EIT: λ19.5nm**

**(c)** **Derived Coronal Holes: Mount Wilson Solar Observatory**

**Transient coronal holes detected by SOHO/EIT.**

**Coronal holes determined by the combined Potential Field Source Surface & Schatten Current Model (PFSS+SCS).**

Figure 2.    Same as Figure 1 but now for CR1922

**(a)** **Solar Wind Speed Predictions & Observations**

**April 10th ICME**

**Stream Source?**

**(b)** **IMF Polarity Predictions & Observations**

**(c)** Coronal Field Polarity (5 Rs)

**(d)** Solar Wind Speed (5 Rs)

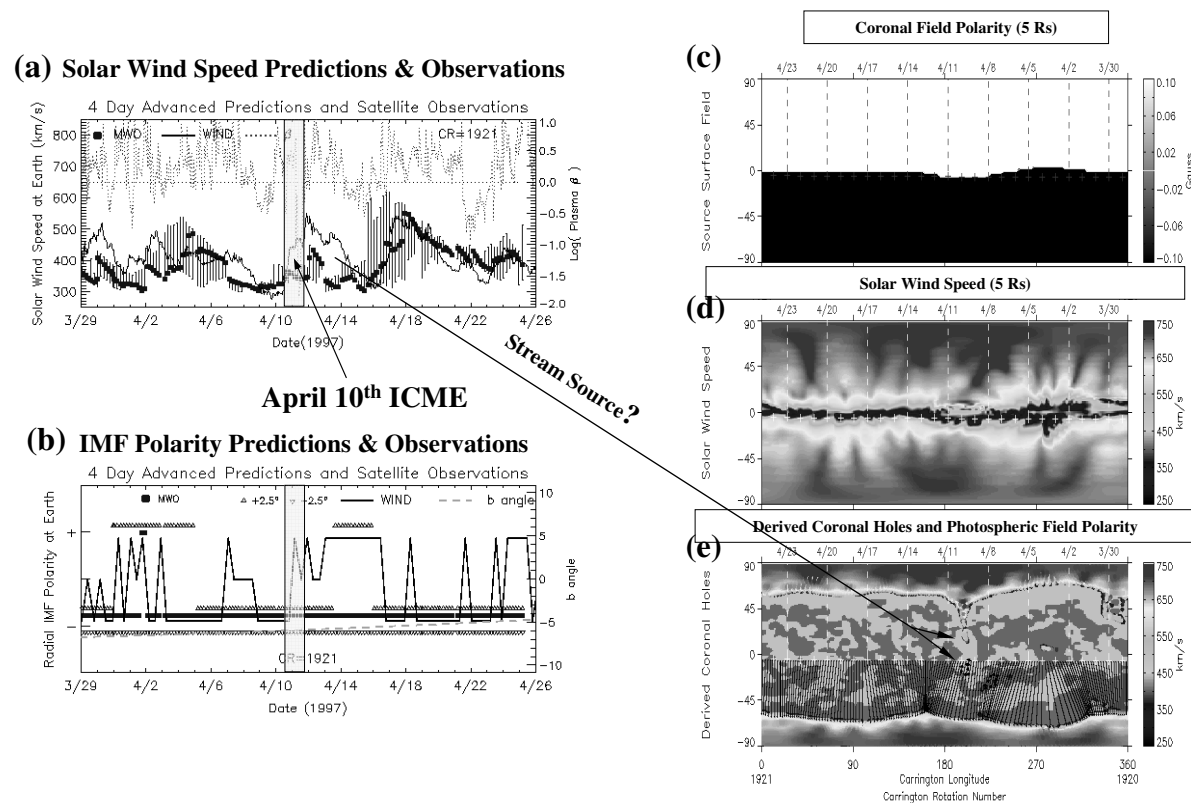**(e)** Derived Coronal Holes and Photospheric Field Polarity

Figure 3. On the right-hand side: (c) the global coronal field polarity at 5Rs , (d) the solar wind speed at 5Rs , and (e) the open field (or coronal hole) configuration at the photosphere. Left-hand side: WSA solar wind speed (a) and IMF polarity (b) predictions versus WIND satellite observations for CR1921. The dashed gray line in 3b is the value of the solar $b$ angle. The arrows identify the stream sources at 5Rs and 1Rs. Note that time runs from right to left in synoptic maps
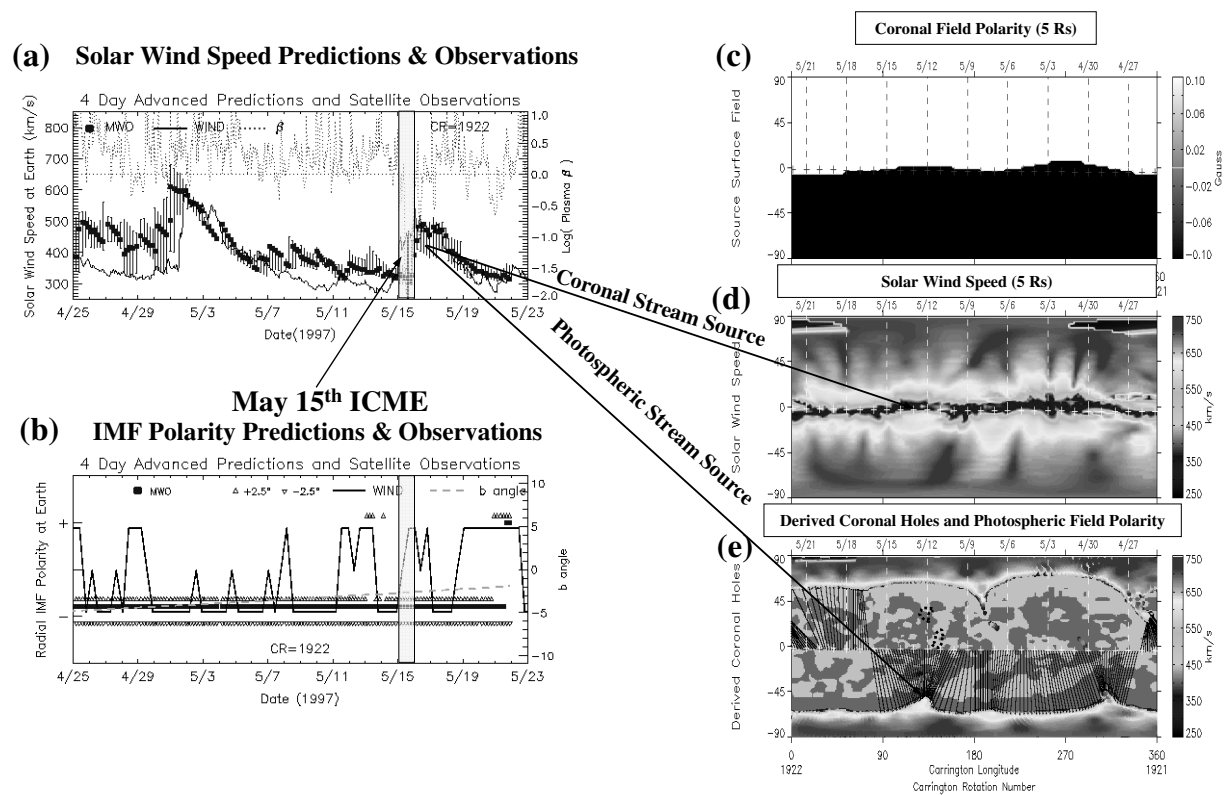
**(a)  Solar Wind Speed Predictions & Observations**

**Coronal Field Polarity (5 Rs)**

**(c)**

**May 15th ICME**

**(b)  IMF Polarity Predictions & Observations**

*Coronal Stream Source*

*Photospheric Stream Source*

**(d)  Solar Wind Speed (5 Rs)**

**(e)  Derived Coronal Holes and Photospheric Field Polarity**

Figure 4.    Same as Figure 3 but now for CR1922

## 3.  Method

In this study, we use daily updated line-of-sight (LOS) photospheric field maps available from MWO as input to the WSA model. The MWO maps have been corrected for line saturation effects using the method developed by Ulrich (1992), have had the LOS field values converted to radial, the polar fields corrected using a procedure described in Arge et. al. (2004), have had any residual monopole moment uniformly removed from each map, and have been converted from their original sine latitude format, with 4° resolution in the longitudinal direction, to ones with uniform 2.5° resolution in both the latitudinal and longitudinal directions.

In Figure 1, we compare the observed coronal hole structure for Carrington Rotation (CR) 1921 (Figures 1a and 1b, which are EUV synoptic maps that we constructed from the original SOHO/EIT 28.4nm and 19.5nm data, respectively) with that predicted by the PFSS and Schatten current sheet (PFSS+SCS) model combination (Figure 1c). The predicted coronal holes in Figure 1c are the tightly spaced gray scale dots (i.e., the open field footpoints at 1Rs, as determined by the model) residing primary north (south) of +50°(-50°) latitude. A narrow coronal hole extension can be seen in the northern hemisphere near ∼200° longitude, extending down to ∼+10° latitude. We have placed the outlines (black lines) of the predicted coronal holes seen in Figure 1c, on top of the EUV images (Figures 1a,b) to help facilitate the comparison. As can be seen, the agreement between the predicted and observed coronal holes is qualitatively, good. Generally speaking, the regions where there appear to be significant discrepancies between the observed and predicted holes (e.g., the area in the northern polar region centered on longitude ∼270° with an angular width of ∼100°) are almost certainly due to bright, high altitude coronal structures lying in between the LOS of the observer and the coronal holes. The reality of the small, isolated coronal holes at lower latitudes is unclear. However, the two small dotted contours found on all of the maps in Figure 1 are the transient twin dimming regions seen clearly in the EIT maps but not predicted by the model. As for CR1921, we find the agreement between the predicted and observed coronal holes for CR1922 (Figure 2) to also be qualitatively good.

In Figure 3a, the solar wind speed observations from the WIND satellite are compared with WSA predictions for CR1921. The vertical bars seen in the figure are uncertainty estimates determined by finding the maximum and minimum values of the predicted solar wind speed at the sub-earth point as well as for those points located 2.5° north and south of them. They therefore provide an estimate of the range over which the solar wind speed can reasonably vary over a 5° latitude range. The black dotted line is the base 10 logarithm of the plasma beta ($\beta$) parameter, which is calculated using the plasma data from the WIND satellite. Small $\beta$ values often indicate the passage of transient solar wind where ambient solar wind models such as WSA are not expected to perform well. We use the $\beta$ parameter here to help with the identification of such transients. In Figure 3b, the solar wind IMF polarity observations from the WIND satellite are compared with WSA predictions for CR1921. The open triangles correspond to IMF polarity predictions for those points located 2.5° in latitude north and south of the sub-earth points. They are analogous to the vertical bars in the solar wind speed plots. When different polarity values are obtained for a given

date and time, the sub-earth point is usually located very near the current sheet. The light gray shaded areas in the two plots correspond to the time-interval of the ICME passage (sheath plus ejecta). Here, as expected, the WSA model fails to capture the transient stream properties. Figures 3c), d), and e) are, respectively, the global coronal field polarity at 5Rs, the solar wind speed at 5Rs (as determined by Eq.1), and the open field (or coronal hole) configuration at the photosphere (identical to Figure 2c). Figure 4 shows the results obtained for CR1922 and has the same format as Figure 3.

## 4.    Discussion

We begin our discussion with the May 12 event. In Figure 4a, we note that the observed and predicted solar wind speeds agree with each other rather well over nearly the entire Carrington rotation, although the model predictions are slightly high from April 25-May 1. The model completely misses the ICME on May 15 (gray shaded area in plot) but then matches the observations remarkably well following its passage. (The WSA model is primarily designed to predict the slowly varying, ambient solar wind and thus does not reproduce ICMEs.) We recently published predictions (Arge et al., 2004) for this same time interval using the identical set of daily updated MWO synoptic maps used here but resolved down to 5° resolution. The agreement between the observed and predicted solar wind speeds is noticeably improved using the 2.5° resolution maps. The IMF polarity predictions (Figure 4b) agree reasonably well with observations over nearly the entire rotation. In those instances where there is disagreement, the source of the problem can almost always be attributed to a combination of two factors: 1) a very flat current sheet and 2) the track of the sun-earth line passing very near the current sheet. The May 11-14 period is a good example of this. Assuming a 5 day propagation time, the coronal source region of this solar wind corresponds roughly to that which left the Sun on May 6-9. As can be seen in Figure 4c, the set of sub-earth points that correspond to this time interval lie right along the current sheet. The source region of the stream that follows the May 15 ICME comes from a coronal hole extension (Figure 4e) in the south, which is consistent with that found by Arge et al. (2004), Odstrcil, Riley, & Zhao (2004) and Odstrcil, Pizzo, & Arge (2005). As in Figures 2a and 2b, we show in Figure 4e the positions of the twin transient coronal holes that were visible during the May 12 event and note that the transient coronal hole with the positive polarity lies very close to the sub-earth point. It may be that the source of the discrepancy between the predicted and observed IMF polarity on May 16 is due to this transient coronal hole. Having composition and abundance data for this period could help resolve this issue.

While the overall agreement between the predicted and observed solar wind speed for CR1921 (see Figure 3a) is reasonable, it is not as good as for CR1922. As one would expect, the model misses the ICME, but significantly, it also misses the stream that follows afterwards. The agreement between the IMF polarity predictions and observations is quiet good, especially when one factors in the flatness of the current sheet (it is even flatter than in CR1922) and the polarity predictions 2.5° north and south of sub-earth points. In all but one case (April 22-25), the model either predicts the observed polarity correctly or

clearly indicates that the sub-earth points lie very near the current sheet (i.e., the predicted IMF values 2.5° north of the sub-earth points have opposite polarity to those for the sub-earth points themselves). The source of the moderate high speed that followed the April 10 ICME is unclear. Our results suggest two possibilities. It could be from one of the two transient coronal holes shown in Figure 3e. One of the holes lies right along the track of the sun-earth line and has a field polarity (positive) consistent with the observations at L1. The WSA model did not predict either of these holes and this could explain why the stream was missed. The other possible source of the stream is the narrow northern coronal extension positioned at ∼200° longitude. It too has a positive field polarity. Figure 3e shows the coronal holes predicted by the WSA model and the connectivity (i.e., black straight lines) between the sub-earth points located on the outer (open) coronal boundary at 5Rs and the source regions of the solar wind at the photosphere. While no connectivity between the transient coronal (with positive polarity) and the sub-earth points is seen, we note that a standard photospheric field Carrington map for CR1921 was used to generate this particular figure (used here primarily for illustrative purposes). However the daily updated maps, which were the synoptic maps actually used to generate the solar wind predictions, did show such a connection. If this coronal hole is the source of the stream, then it is unclear exactly why the model missed it. One important difference between this coronal hole and the one from the May 12 event, is that it had an active region positioned near its southern-most end. The only active region in the May 12 event was located in the north, while the source region for the stream that followed the May 15 ICME was in the south. It is well known that active regions are non-potential and this may explain why the model missed the stream. We also considered the possibility that the polar field correction applied to the maps was not entirely correct. For example, if the polar fields were too strong, the coronal extension, as determined from the model, would very likely be too small and narrow. In this case, our empirical solar wind relationship could have under-predicted the speed (since it is a function of $\theta_b$ as well as $f_s$) of the solar wind emerging from this hole. To test this hypothesis, we both increased and decreased the polar fields of the daily updated maps by 20%. We find that this did not make a significant difference in the solar wind predictions. Another possibility is that our empirical solar wind speed relationship needs to be modified for solar wind sources that are near active regions. We need to investigate this possibility further.

## 5.   Summary

We have modeled the ambient solar wind during the times of the April 7 and May 12 1997 CMEs using the WSA model. We find that the model describes the observed ambient solar wind stream structure around the time of the May 12 CME generally well, except for the ejecta itself. The model suggests that the source of the high-speed stream that followed and compressed the May 12th CME from behind originated from a small coronal hole extension located south of the Sun's equator. For the April 7 event, the model missed both the ejecta and the stream that followed behind it. There are at least four possibilities for why the stream was missed. The coronal hole extension located in the northern

hemisphere may be the stream's source and 1) the polar fields in the daily updated photospheric field maps were not corrected properly, or 2) the source region of the stream lies near an active region, which is likely non-potential. We both increased and decreased the polar field strengths of the daily updated maps by 20% and found no significant change in the solar wind predictions, thus (seemly) ruling out the first of these two possibilities. The third reason why the stream following the May 15 ICME may have been missed is because its source was one of the transient coronal holes associated with the April 7 CME. Having composition and abundance data for this period could help rule this possibility in or out. A final possibility may be that we need to modify our empirical solar wind speed relationship when the solar wind source region is near an active region.

## References

Altschuler, M., & Newkirk Jr., G. 1969, Solar Phys., 9, 131

Arge, C. N., Luhmann, J. G., Odstrcil, D., Schrijver, C. J., Li, Y. 2004, J. Atm. & Solar-Terres. Phys., 66, 1295

Arge, C. N., Harvey, K. L., Hudson, H. S., & Kahler, S. W. in AIP Conf. Proc. 679, Solar Wind Ten: Proceedings of the Tenth International Solar Wind Conference, (New York: AIP), 202

Arge, C., & Pizzo, V. 2000, JGR, 105, 10465

Berdichevsky, D., Bougeret, J.-L., Delaboudinihre, J.-P., Fox, N., Kaiser, M., Lepping, R., Michels, D., Plunkett, S., Reames, D., Reiner, M., Richardson, I., Rostoker, G., Steinberg, J., Thompson, B., & von Rosenvinge, T. 1998, GRL, 25, 2473

Odstrcil, D., Pizzo, V., & Arge, C. 2005, JGR, 110, A02106

Odstrcil, D., Riley, P., & Zhao, X. 2004, JGR, 109, A02116

Plunkett, S. P., Thompson, B. J., Howard, R. A., Michels, D. J., St. Cyr, O. C., Tappin, S. J., Schwenn, R., & Lamy, P. L. 1998, GRL, 25, 2477

Schatten, K. 1971, Cosmic Electrodyn., 2, 232

Schatten, K., Wilcox, J., & Ness, N. 1969, Solar Phys., 9, 442

Ulrich, R. 1992. in ASP Conf. Ser. Vol. 26, Cool Stars, Stellar Systems, and the Sun, ed. M. S. Giampapa, & J. A. Bookbinder (San Francisco: ASP), 265

Wang, Y., & Sheeley, N., Jr. 1992, ApJ, 392, 310

Webb, D. F., Cliver, E. W., Crooker, N. U., Cry, O. C. St., & Thompson, B. J. 2000a, JGR, 105, 7491

Webb, D. F., Lepping, R. P., Burlaga, L. F., DeForest, C. E., Larson, D. E., Martin, S. F., Plunkett, S. P., & Rust, D. M. 2000b, JGR, 105, 27251